The Astrophysical Journal, 636:881–890, 2006 January 10
Copyright is not claimed for this article. Printed in U.S.A.

STARBURST MODELS FOR FAR-INFRARED/SUBMILLIMETER/MILLIMETER LINE EMISSION. I. AN EXPANDING SUPERSHELL SURROUNDING A MASSIVE STAR CLUSTER

Lihong Yao
Department of Astronomy and Astrophysics, University of Toronto, Toronto, ON M5S 3H8, Canada; yao@astro.utoronto.ca

T. A. Bell, S. Viti, and J. A. Yates
Department of Astronomy and Astrophysics, University College London, London WC1E 6BT, UK

and

E. R. Seaquist
Department of Astronomy and Astrophysics, University of Toronto, Toronto, ON M5S 3H8, Canada
Received 2005 July 22; accepted 2005 September 19

ABSTRACT

The effect of a newly born star cluster inside a giant molecular cloud (GMC) is to produce a hot bubble and a thin, dense shell of interstellar gas and dust swept up by the H II expansion, strong stellar winds, and repeated supernova explosions. Lying at the inner side of the shell is the photodissociation region (PDR), the origin of much of the far-infrared/submillimeter/millimeter (FIR/submm/mm) radiation from the interstellar medium (ISM). We present a model for the expanding shell at different stages of its expansion that predict mm/submm and far-IR emission line intensities from a series of key molecular and atomic constituents in the shell. The kinematic properties of the swept-up shell predicted by our model are in very good agreement with the measurements of the supershell detected in the nearby starburst galaxy M82. We compare the modeling results with the ratio-ratio plots of the FIR/submm/mm line emission in the central 1.0 kpc region to investigate the mechanism of star-forming activity in M82. Our model has yielded appropriate gas densities, temperatures, and structure scales compared to those measured in M82, and the total H_2 content is compatible with the observations. This implies that the neutral ISM of the central star-forming region is a product of fragments of the evolving shells.

Subject headings: galaxies: ISM — galaxies: starburst — ISM: clouds — ISM: evolution — ISM: molecules — stars: formation

1. INTRODUCTION

Starburst is a phenomenon that occurs when the star formation rate (SFR) cannot be sustained for the lifetime of the galaxy. It is now clear that active star formation or starburst activity is common throughout the universe (Madau et al. 1998). The bursts of massive star formation can dramatically alter the structure and evolution of their host galaxies by injecting large amounts of energy and mass into the ISM via strong stellar winds and repeated supernova explosions. The evolution of the superbubbles and supershells that have sizes ranging from several tens to hundreds of parsecs plays an important role in understanding the amount and distribution of warm gas in the ISM. Furthermore, understanding the characteristics of starbursts and their relationship with the ISM, as well as being able to parameterize the star formation history, are crucial in understanding the galaxy evolution.

In the past, several models have been used to interpret the infrared, submillimeter, and millimeter line observations of neutral gas in the central regions of nearby starburst galaxies (e.g., Mao et al. 2000; Seaquist & Frayer 2000; Wild et al. 1992 and references therein). These include the large velocity gradient (LVG) model (Goldreich & Kwan 1974), the steady state PDR model (Tielens & Hollenbach 1985), and the inhomogeneous radiative transfer model taking into account non–local thermodynamic equilibrium (non-LTE; Wild et al. 1992). These have revealed that the physical conditions (such as gas density, FUV flux, and gas kinetic temperature) are enhanced in starburst regions. However, none of these models are able to relate the observed line emission properties of the neutral gas in a starburst galaxy to its age and star formation history. In this paper, we introduce an evolving starburst model for FIR/submm/mm line emission in gas media that allows us to ultimately achieve this goal.

Our model consists of a standard dynamical model of the bubble/shell structure around a young star cluster (see Fig. 1), which has been described in many publications (e.g., Castor et al. 1975; Weaver et al. 1977; McCray & Kafatos 1987; Franco et al. 1990; Koo & McKee 1992); a time-dependent stellar population synthesis model (Leitherer et al. 1999); a fully time-dependent PDR chemistry model (Bell et al. 2005); and a one-dimensional non-LTE line radiative transfer model (Rawlings & Yates 2001). In this paper, we conduct a preliminary study using this set of models. We first describe the methodology of our model (§ 2). We then follow the evolution of a GMC and a swept-up shell induced by massive star formation at the center and calculate the dynamics, thermal structure, and the line radiative transfer of the selected molecular and atomic species in the expanding shell (§ 3). We compare our modeling results with the observations of the expanding supershell and average gas properties in the central 1.0 kpc region of the nearby starburst galaxy M82 (§ 4). Finally, we present the conclusions of this study (§ 5).

The basic assumptions for our evolving starburst model are as follows: (1) star formation occurs primarily within the dense, optically thick spherical cloud (e.g., Gao et al. 2001), and all stars form instantaneously in a compact spherical cluster located at the center of the cloud (the star cluster is therefore treated as a point source); and (2) the starlight produced by the central cluster is completely absorbed and reprocessed by the dust in the expanding

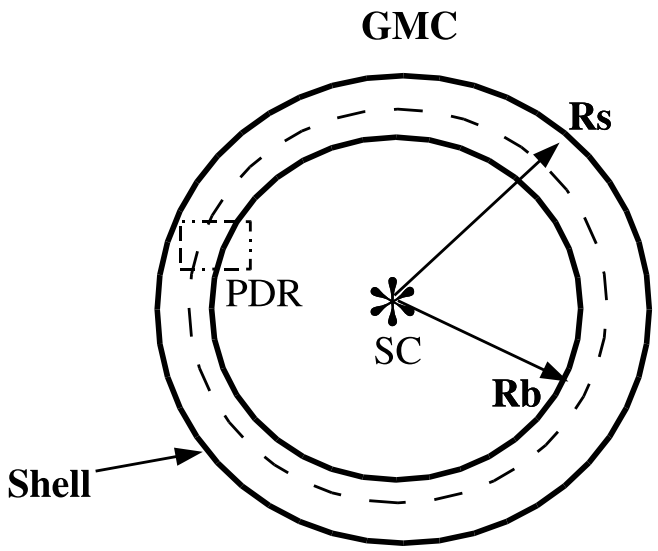

FIG. 1.—Schematic structure of an evolving GMC centrally illuminated by a compact young star cluster (SC); R_s is the radius of the shell, and R_b is the radius of the bubble. The PDR lies between the thin, dense swept-up shell and the interior (Hollenbach & Tielens 1997).

shell (Efstathiou et al. 2000). A summary of our evolving starburst model is presented in Table 1.

TABLE 1
SUMMARY OF STARBURST MODELS FOR FIR/submm/mm LINE EMISSION

Name and Description
Assumptions
Spherical geometry, nonmagnetized (GMCs and shells)
No interactions between shells, or between shell and cloud
Dustless H II regions
Uniform densities of GMCs and ambient media
All stars form instantaneously; no stars form inside the shells
Stellar mass 0.1–120 $M_\odot$ with Salpeter IMF $dN/dM_* \propto M_*^{-2.35}$
PDRs exist primarily within the expanding shells
Input Parameters
GMC mass $M_{\rm GMC} = 10^7\ M_\odot$
Average cloud density $n_0 = 300$ cm^{-3}, cloud core density $n_c = 2000$ cm^{-3}
Ambient ISM density $n_{\rm ISM} = 30$ cm^{-3}
Star formation efficiency $\eta = 0.25$
Metallicity $\mathcal{Z} = 1.0\ Z_\odot$
Gas-to-dust ratio = 100
Output Parameters
Radius, velocity, temperature, density, and thickness of the shell
Chemical abundances of different molecules and atoms in the shell
Integrated line intensity/flux, line ratios
Observational
Line intensities/fluxes and line ratios for molecules (e.g., ^{12}CO, ^{13}CO, HCN, and HCO$^+$) and atoms (e.g., [C I], [C II], and [O I])

NOTE.—See also Table 2 for more input parameters for the time-dependent PDR model.

2. STARBURST MODELS FOR GAS MEDIA

The evolution of a giant molecular cloud is determined by H II expansion in the very early stage ($t < 10^5$ yr), when a hot bubble surrounded by a thin, dense shell structure is created. The later evolution is driven by the strong stellar winds and repeated supernova explosions. We assume that repeated supernova explosions behave like a steady isotropic stellar wind injected into the bubble. The hot bubble will eventually cool, and the swept-up shell will stall after a few times 10^7 yr. The stars in the young cluster located at the center of the GMC are assumed to have masses between 0.1 and 120 $M_\odot$. The Salpeter initial mass function (IMF) $dN/dm_* \propto m_*^{-2.35}$ (Salpeter 1955) is adopted in this study. A top-heavy IMF, which has an excess of stars in the mass range 10–20 $M_\odot$ over stars of 5 $M_\odot$ or less for starburst galaxies (e.g., Rieke et al. 1980), will be investigated in future work.

2.1. *Shell Dynamics*

The radius and velocity of the H II *expansion* due to ionization can be written as (Spitzer 1978; Franco et al. 1990)

$$R_{\rm H\,II}(t) = R_{\rm S}\left(1 + \frac{7}{4}\frac{c_i t}{R_{\rm S}}\right)^{4/7}, \tag{1a}$$

$$V_{\rm H\,II}(t) = c_i\left(1 + \frac{7}{4}\frac{c_i t}{R_{\rm S}}\right)^{-3/7}, \tag{1b}$$

where $R_{\rm S}$ is the initial Strömgren radius in parsecs, and $c_i \simeq 11.5$ km s^{-1} is the sound speed in the ionized gas with an equilibrium temperature of $\sim 10^4$ K.

Almost as soon as the initial Strömgren sphere is formed, the strong winds start to impart large amounts of mechanical energy into the bubble. About 96% of the total wind energy is generated by stars with masses >30 $M_\odot$ (McCray & Kafatos 1987). The size of the hot bubble is assumed to be much larger than the thickness of the swept-up shell; therefore, the radius and velocity of the shell in the *winds* phase can be written as (McCray & Kafatos 1987)

$$R_w(t) = 269.0\left(\frac{L_{38}}{n}\right)^{1/5}(t_7)^{3/5}, \tag{2a}$$

$$V_w(t) = 16.1\left(\frac{L_{38}}{n}\right)^{1/5}(t_7)^{-2/5}, \tag{2b}$$

where $L_{38} = L_w/(10^{38}$ ergs s$^{-1})$, L_w is the wind mechanical luminosity, $L_w = \int_{m_1}^{m_2} C_w C_m m_*^{\gamma-2.35}\, dm_*$, $t_7 = t/(10^7$ yr), n is the ambient gas density in cubic centimeters, $m_1 = 0.1\ M_\odot$, $m_2 = 120\ M_\odot$, $C_w = 1.0 \times 10^{29}$, $C_m = 429.0$, and $\gamma = 3.7$ (derived from Abbott 1982). The main-sequence lifetime of the most massive star (120 $M_\odot$) in the star cluster is about 7.0×10^5 yr (Mac Low & McCray 1988). After this time, we assume that the wind equivalent energy produced by the first supernova and the subsequent ones drives the further expansion of the swept-up shell. The radius and velocity of the shell in the *supernova* phase can be written as

$$R_{\rm SN}(t) = 97.0\left(\frac{N_* E_{51}}{n}\right)^{1/5}\left[(t_7)^{3/5} - \left(\frac{t_{\rm 1st\,SN}}{10^7}\right)^{3/5}\right] + R_w(t_{\rm 1st\,SN}), \tag{3a}$$

$$V_{\rm SN}(t) = 5.7\left(\frac{N_* E_{51}}{n}\right)^{1/5}(t_7)^{-2/5}, \tag{3b}$$

where N_* is the number of stars with masses $\geq 8\ M_\odot$ in the cluster, $E_{51} = E_{\rm SN}/(10^{51}$ ergs s$^{-1})$, $E_{\rm SN}$ is the energy produced by

each supernova explosion, $t_{1\mathrm{st\,SN}}$ is the time when the first supernova occurs in the star cluster, and $R_w(t_{1\mathrm{st\,SN}})$ is the shell radius at $t_{1\mathrm{st\,SN}}$ calculated from equation (2a). The average rate of supernova explosions is $\sim 6.3 \times 10^{35} N_* E_{51}$ ergs s^{-1} (McCray & Kafatos 1987). When the energy produced by the stellar winds and/or supernova explosions is much greater than the radiative losses, the bubble is adiabatic. This *adiabatic* phase persists until the radiative cooling becomes important for the hot bubble at t_c,

$$t_c = 4 \times 10^6 Z^{-15} (N_* E_{51})^{3/10} n^{-7/10}, \tag{4}$$

where Z is the metallicity with respect to the solar. After t_c, the expansion of the bubble is no longer energy-driven, but momentum-driven. This momentum-driven phase is characterized as the *snowplow* (SP) phase. For simplicity, we ignore the momentum deposition in the shell by supernova (SN) ejecta (McCray & Kafatos 1987). Hence, the radius and velocity of the shell in the snowplow phase can be written as

$$R_{\mathrm{SP}}(t) = R_c \left(\frac{t}{t_c}\right)^{1/4}, \tag{5a}$$

$$V_{\mathrm{SP}}(t) = \frac{R_c}{4t_c} \left(\frac{t}{t_c}\right)^{-3/4}, \tag{5b}$$

where R_c is the radius of the bubble at cooling time t_c. The snowplow phase ends when the shell expansion velocity is close to the thermal sound speed of gas in the ISM (typically ~ 10 km s^{-1}). The shell will stall and disperse due to the Rayleigh-Taylor instability (Mac Low 1999).

Our one-dimensional shell dynamical model may overestimate the wind and supernova mechanical luminosities, as argued recently by Dopita et al. (2005), because the mixing and dynamical instabilities occur in two dimensions, and the ISM is intrinsically inhomogeneous. Dopita et al. (2005) also suggested that the higher ISM pressure in starburst regions causes the expanding shell to stall at a smaller radius. Another argument is that the gravitational instability may induce new star formation inside the shells. These concerns may indicate that the conventional bubble/shell dynamics (Weaver et al. 1977; McCray & Kafatos 1987) may need to be modified.

2.2. *Physical Conditions of the Swept-up Gas*

The PDRs that lie at the inner sides of the clouds or shells centrally illuminated by massive star formation are the origin of much of the FIR/submm/mm radiation from the ISM. Physical conditions of the swept-up gas in these PDRs are very different from those of the cold gas components in the ISM. The gas temperature and density of the swept-up shells are a few orders of magnitude higher due to the strong FUV radiation and shock compression. The FUV radiation (6 eV $< h\nu <$ 13.6 eV) produced by newborn stars plays an important role in the heating and chemistry of PDRs, especially during the early evolution. Other sources that may contribute to the shell heating are the mechanical energy input by winds and SN explosions (McKee 1999), shocks caused by the accretion of gas at the outer surface of the shell (McKee & Hollenbach 1980), and cosmic rays (Suchkov et al. 1993; Bradford et al. 2003). Cosmic rays may play an important role in the heating of swept-up gas after the stars with masses $\geq 8\ M_\odot$ have terminated as supernovae. Heating sources due to cloud-cloud collisions (McCray & Snow 1979) or shell-shell interaction (Scalo & Chappell 1999) are not considered in this study.

The total FUV flux is calculated by integrating the flux of the stellar population spectrum between 912 and 2055 Å for each time step using Starburst99, a time-dependent stellar population synthesis model developed by Leitherer et al. (1999). We consider an instantaneous burst for the star formation law, where the star formation occurs all at the same time (i.e., at age zero). The FUV field strength G_0 incident on the inner surface of the shell (visual extinction $A_V = 0$) is then calculated by taking the ratio of the total FUV flux to the surface area $4\pi r_s^2(t)$ of the expanding shell at each time step. We use the same input parameters and assumptions for Starburst99 as those used in the shell dynamics calculation (see Table 1).

The swept-up shell itself is supported by thermal gas pressure and nonthermal pressure due to microturbulence. The gas temperature decreases toward the outer surface of the shell, and the total gas density is assumed uniform. Therefore, the pressure is lower at the outer surface. The shell density n_s refers to the total H_2 density $n(H_2)$ in this study. The shell density at each time step is derived from balancing the pressure at the outer surface of the shell with the ram pressure,

$$n_s(t) = \frac{n_a v_s^2(t)}{kT_s(t)/\mu + \delta v_D^2}, \tag{6}$$

where n_a is the ambient molecular gas density, $v_s(t)$ is the expansion velocity, $T_s(t)$ is the gas temperature at the outer surface of the shell, μ is the mean molecular weight, $\mu = 0.62 m_{\mathrm{H}}$, m_{H} is the mass of the hydrogen atom, and δv_D is the microturbulent velocity inside the shell. The calculation of the gas temperature profile across the shell is described in § 2.3. The thickness of the shell d_s at each time step is in turn calculated using the continuity equation (or mass conservation law),

$$d_s(t) = \frac{n_a r_s(t)}{3 n_s(t)}. \tag{7}$$

2.3. *The Time-dependent PDR Model*

The gas temperature and chemical abundances of the swept-up shell are calculated self-consistently at each depth and time step, using the time-dependent PDR model developed at University College London (UCL) (called UCL_PDR). A fully time-dependent treatment of the chemistry is employed in UCL_PDR that includes 128 species involved in a network of over 1700 reactions (Bell et al. 2005 and references therein). The polycylic aromatic hydrocarbons (PAHs) chemistry is not included. The reaction rates are taken from the UMIST chemical database (Le Teuff et al. 2000). Detailed chemical modeling, heating and cooling mechanisms, and the thermal balance between them are described in the literature (e.g., Taylor et al. 1993; Papadopoulos et al. 2002 and references therein). Heating due to shocks is not included. The UCL_PDR code has been modified for the purpose of this study to include a pressure balance check at the outer surface of the shell, as well as the evolution information of shell density, thickness, and FUV radiation strength.

The UCL_PDR code assumes a plane-parallel geometry and models the PDR as a semi-infinite slab of homogeneous density at a given time step. The pressure is thus not in equilibrium across the PDR region. The FUV radiation field illuminates the shell from one side, and it becomes attenuated with increasing visual extinction A_V into the shell at a given time step as $G = G_0 e^{-2.4 k A_V}$, where G_0 is the FUV strength at $A_V = 0$ calculated by the Starburst99 model. The coefficient $2.4k$ in front of the A_V in the exponent takes into account the difference in opacity from

the visible to the UV and the influence of grain scattering. The timescale for gas in PDRs to reach chemical equilibrium depends on the gas density, temperature, degree of ionization, and species involved (Hollenbach & Tielens 1997; van Dishoeck & Blake 1998). In our study, this timescale varies from 10^5 to 10^7 yr for the swept-up gas. Our comparative tests using a single time step model fail to reproduce important chemical structure features predicted by the fully time-dependent model for ages up to 10 Myr. The use of a fully time-dependent PDR code in which temperature and density changes with time is therefore justified in modeling the shell evolution over these timescales.

2.4. *The Non-LTE Line Radiative Transfer Model*

The line radiative transfer properties are calculated using the Spherical Multi-Mol (SMMOL) code. The SMMOL model was also developed at UCL, implementing an accelerated Λ-iteration (ALI) method to solve multilevel non-LTE radiative transfer problems of gas inflow and outflow. The code computes the total radiation field and the level populations self-consistently. At each radial point, SMMOL generates the level populations and the line source functions. Our model assumes that the gas emission originates in the unresolved, homogeneous, spherical expanding shell, and that all gas and dust in the H II region have been swept up into the shell, i.e., a dustless H II region. The background radiation field is assumed to be the cosmic background continuum of 2.73 K. A detailed description of the SMMOL radiative transfer model and its implementation can be found in the appendix of Rawlings & Yates (2001). The benchmarking and comparison with other line radiative transfer models are presented in van Zadelhoff et al. (2002).

Several programs were developed to separate and extract the gas temperature and fractional abundances for molecular and atomic species calculated by the UCL_PDR code. These extracted gas temperature and abundances, along with the shell density, thickness, radius, and expansion velocity computed by the dynamical code, are regridded for a spherical geometry and used as input parameters for the SMMOL code to compute the total line intensity or flux. Einstein A- and collisional rate coefficients for the molecular and atomic lines are taken from the Leiden Atomic and Molecular Database (Schöier et al. 2005). The lowest 10 energy levels are calculated for all molecules: three for atomic [C I] and [O I], and eight for atomic [C II].

3. SIMULATION OF AN EXPANDING SHELL

Observational studies have shown that molecular clouds in the Milky Way have a distinct mass spectrum $M^{\alpha}_{\rm GMC}$, with $\alpha = -1.5 \pm 0.1$ (Sanders et al. 1985; Solomon et al. 1987) for cloud masses ranging between 10^2 and $10^7\ M_\odot$. Therefore, about 70% of the molecular mass in the Galaxy is contained in the GMCs with masses $>10^6\ M_\odot$. These giant molecular clouds are known to be associated with active formation of massive stars. If we assume that the cloud mass distribution in a starburst galaxy follows an index similar to the Galactic one, we would expect much of the luminosity of the starburst to arise from the GMCs with a fairly narrow range of masses. We adopt a value for the cloud mass of $10^7\ M_\odot$ for the GMCs in this study. We assume the average gas consumption rate or star formation efficiency η in starburst galaxies per 10^8 yr to be 0.25 (Kennicutt 1998). Therefore, the total stellar mass M_* for the star cluster in the center of the GMC is $2.5 \times 10^6\ M_\odot$, and the number of stars N_* with masses $m_* \geq 8\ M_\odot$ is about 2.2×10^4. The radius of the GMC is about 50 pc, with an average cloud density $n_0 = 300\ {\rm cm}^{-3}$ and a cloud core density $n_c = 2 \times 10^3\ {\rm cm}^{-3}$ (Plume et al. 1992; Efstathiou et al. 2000). The ambient density $n_{\rm ISM}$ is assumed to be 30 cm^{-3} (Comeron & Torra 1994). Here we present an idealized case study with this particular set of input parameters.

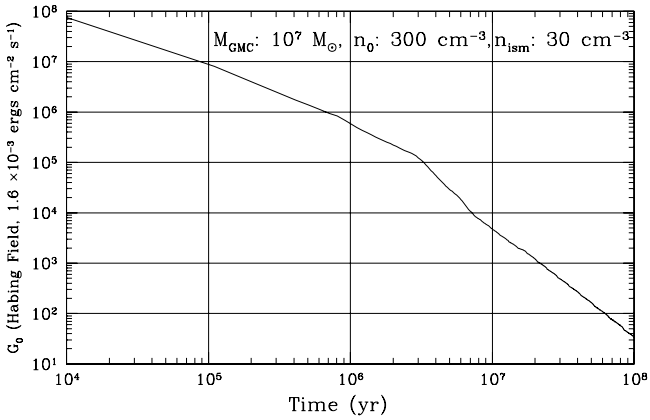

FIG. 2.—Plot of the FUV radiation field strength G_0 incident on the inner surface of the shell ($A_V = 0$) as a function of time (see text for details).

3.1. *Kinematics of the Swept-up Gas*

The size of the H II region increases slowly with time. The Strömgren radius is about 4.9 pc, assuming the number of Lyman continuum photons is 5×10^{52} s^{-1}. The wind bubble catches up with the H II ionization front in a time less than 10^5 yr. The strong stellar winds cause the bubble to expand quickly into the cloud and sweep up more gas into the shell. The total wind power is estimated as $L_w \simeq 1.4 \times 10^{40}$ ergs s^{-1} for the star cluster used in the model. When the most massive star in the center cluster ($120\ M_\odot$) terminates as a supernova at ~0.7 Myr, the thin shell caused by the H II region expansion and the stellar winds is still expanding at a speed of ~40 km s^{-1}. At this time, the shell has swept up much of the mass of its parent cloud and is propelled into the ISM with a uniform density. The mechanical energy produced by the first supernova and the subsequent ones reenergizes the shell. A supernova cutoff mass of $8\ M_\odot$ is assumed. The total energy generated by supernova explosions is $\sim 2.0 \times 10^{55}$ ergs over 40 Myr. At ~7.5 Myr, the hot bubble starts to cool and loses its internal pressure, at which time the adiabatic phase ends. We adopt 1.0 for the metallicity $\mathcal{Z}$ with respect to the solar throughout this study. The effect of lower metallicity, which is suspected to be present in starburst galaxies, will be discussed in a future paper. The radius and velocity of the shell at the end of the adiabatic phase are about 270 pc and 24 km s^{-1}, respectively. At ~50 Myr, the expansion velocity of the shell decreases to ~10 km s^{-1}, and the shell stalls and becomes thicker and less dense.

Figure 2 shows the FUV radiation strength G_0 incident on the inner surface of the shell ($A_V = 0$) as a function of time. The G_0 value is in units of the Habing field, that is, 1.6×10^{-3} ergs cm^{-2} s^{-1} throughout this study. The FUV strength decreases from about 10^8 to 10^5 from the onset of star formation to about 5 Myr when most of the massive O stars ($>30\ M_\odot$) have terminated as supernovae. It then decreases twice as fast to a value of 40 at 100 Myr.

PDRs are the origin of much of the FIR/submm/mm line emission in a starburst galaxy. The surface layer ($A_V \sim 1$) contains atomic H, C, C^+, and O; the transition from atomic to molecular hydrogen occurs at the center layer ($A_V \sim 1$–2), while C^+ is converted into C and then CO over the region $A_V \sim 2$–4. H_2 and CO then extend to a higher A_V region, and for $A_V > 10$ atomic O begins to be transformed into molecular O_2. The H_2 molecule provides effective self-shielding from the FUV radiation

TABLE 2
INPUT PARAMETERS FOR THE TIME-DEPENDENT PDR MODEL

Parameter	Symbol	Value
Starburst age (yr)	t	$0 \leq t < 10^8$
Incident FUV flux (Habing field)	G_0	$10 < G_0 \leq 10^8$
Turbulent (microturbulence) velocity (km s^{-1})	δv_D	1.5
PDR surface density ($A_V = 0$ mag)	$n_{\rm H}$	$10^3 \leq n_{\rm H} < 10^7$
PAH abundance	$x_{\rm PAH}$	4.0×10^{-7}
Dust visual absorption cross section (cm^{-2})	σ_v	3.1×10^{-10}
H_2 formation rate on dust at $A_V = 0$ (cm^3 s^{-1})	$\eta_{\rm H_2}$	3.0×10^{-18}
Cosmic-ray ionization rate (s^{-1})	ζ	1.3×10^{-17}

NOTE.—The initial gas-phase abundances relative to H for all depths at the first time step ($t = 0$ yr) are produced by a single-point, dense, dark cloud model (see text for details).

field. The CO layer also shows a degree of self-shielding and therefore extends deeper into the shell. Small grains play an important role in the photoelectric heating of PDRs. Gas heating is dominated by collisional deexcitation of FUV-pumped H_2 and vibrationally excited H_2 at the PDR surface. The thermal energy radiated by the dust is important for the gas heating at larger optical depth (Hollenbach et al. 1991). The gas heating/chemistry at later evolutionary stages is no longer dominated by stellar radiation but by other sources, such as cosmic rays and X-rays. The PDR cooling is dominated by fine-structure line emission, such as the [C II] 158 μm and [O I] 63 μm transitions, whose critical densities are 3×10^3 and 5×10^5 cm^{-3}, respectively. At greater depths, molecular line emission (CO, OH, and H_2O), rovibrational transitions of H_2, and gas-dust collisions contribute to the PDR cooling.

Table 2 summarizes the input parameters for our fully time-dependent PDR model. The initial abundance of H_2 is set to $n({\rm H_2})/n_{\rm H} = 0.5$ (Hartquist et al. 2003). At the first time step ($t = 0$ yr), all depth steps take as their initial abundances the values produced by a single-point, dense, dark cloud model. The input parameters for the dark cloud modeling are $n_{\rm H} = 4 \times 10^5$ cm^{-3}, $T_{\rm GMC} = 10$ K, and $G_0 = 1$; and the gas-phase abundances relative to H nuclei are $x_{\rm He} = 7.5 \times 10^{-2}$, $x_{\rm C} = 1.8 \times 10^{-4}$, $x_{\rm O} = 4.4 \times 10^{-4}$, and $x_{\rm Mg} = 5.1 \times 10^{-6}$. For subsequent time steps, the input abundances are reset to the output abundances of the previous time step generated by the UCL_PDR code. The gas temperature and chemical abundances at each depth and time step are calculated by balancing the heating and cooling. The cosmic-ray ionization rate is enhanced by a factor of 1.5 at later times ($t > 10$ Myr) to artificially include the soft X-ray heating effect on the gas of the shell. We assume that the gas-to-dust mass ratio is 100. Figure 3 shows the shell density n_s [or $n({\rm H_2})$] and thickness d_s as a function of time, as calculated by the shell dynamical code and the UCL_PDR code, under the condition that the gas pressure at the outer surface of the shell differs from the ambient gas pressure by $\leq$10%. The shell density varies between 10^3 and 10^6 cm^{-3}, and the thickness of the shell changes from 10^{-3} to 10 pc over the 100 Myr. We adopt a fixed microturbulent velocity $\delta v_D = 1.5$ km s^{-1} for the shell. The evolution of the shell density and thickness is constrained by the expansion velocity v_s, the shell temperature T_s, and the ambient density n_a (See eqs. [6] and [7]). Changes in v_s and T_s are relatively small during the H II expansion ($n_a = n_0$ or 300 cm^{-3}); as a result we see the first plateau, as shown in Figure 3. The jump seen at $t \sim 2 \times 10^4$ yr is caused by the change from the H II expansion to the *winds* phase. During the early *winds* phase and before the shell sweeps up all the material of its parent GMC ($t < 0.8$ Myr), the effect due to the shell deceleration is compensated for the effect due to the cooling in the shell. This produces a second plateau. After this time, the shell expands into a less dense ambient ISM, i.e., $n_a = n_{\rm ISM}$ or 30 cm^{-3}. Less ambient pressure causes a decrease in the shell density or an increase in the shell thickness. Figures 4 and 5 show the profiles of the gas temperature and chemical abundances as a function of visual extinction A_V for an expanding shell at several characteristic ages. The size of the PDR changes with time indicated by different maximum values of A_V in both Figures 4 and 5. At $\sim$0.7 Myr, all mass in the GMC has been swept into the shell.

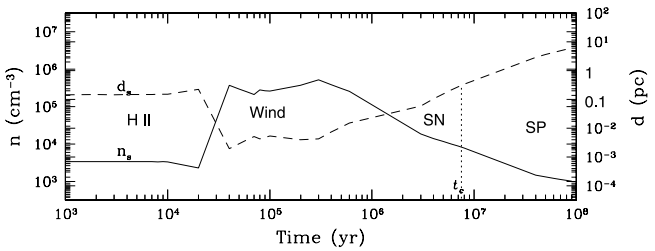

FIG. 3.—Plot of the shell density [n_s or $n({\rm H_2})$, *solid line*] and thickness (d_s, *dashed line*) as a function of time for $M_{\rm GMC} = 10^7\ M_\odot$, an initial cloud density $n_{\rm GMC} = 300$ cm^{-3}, and an ambient ISM density $n_{\rm ISM} = 30$ cm^{-3}. The radiative cooling of the hot interior occurs at $t_c \simeq 7.5$ Myr (*dotted line*). Data for n_s and d_s after 10^4 yr shown in the plots have been smoothed.

3.2. *Molecular and Atomic Line Emission*

The flux and intensity of FIR/submm/mm line emission is calculated for several molecular and atomic species (CO, HCN, HCO^+, C, C^+, and O). The total flux or intensity of each line is the sum of the emission from the entire shell. For the initial 0.7 Myr, the emission from the parent GMC is also taken into account in the total line emission calculation. In this section, we present predictions of the line ratios for CO, [C I], and [C II] for an expanding shell. More simulations will be presented and discussed when we illustrate the model by a comparison with the observations of M82 in § 4.

Molecular CO is known as a good tracer for the diffuse components and total molecular gas content in a galaxy, but it is a relatively poor tracer of the dense gas directly involved in massive star formation. Figure 6 shows our modeling results for line ratios of high-J transitions to the 1–0 transition of the bright and highly abundant ^{12}CO molecule as a function of the starburst age of the shell:

$$r_{21} = I_{21}/I_{10},$$

$$\vdots$$

$$r_{71} = I_{76}/I_{10},$$

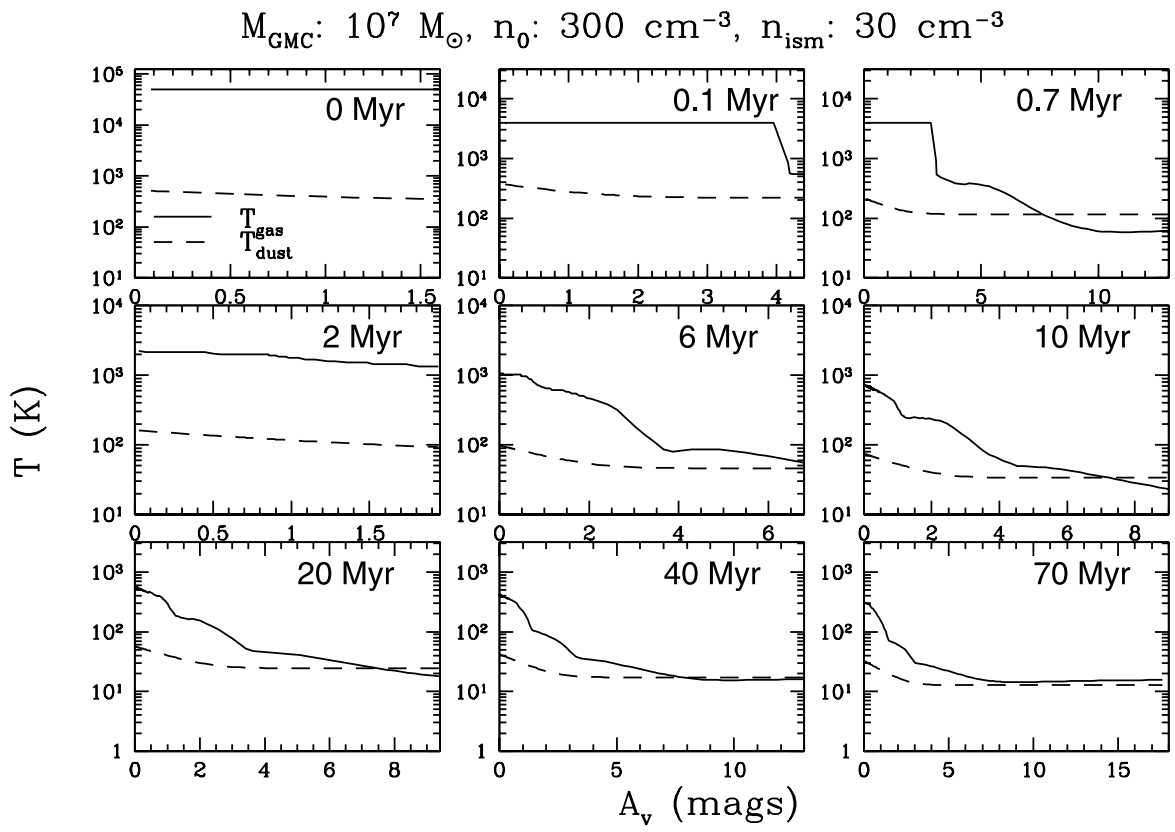

FIG. 4.—Time-dependent gas and dust temperatures as a function of visual extinction A_V for an expanding shell. Solid lines represent gas temperature, and dashed lines indicate dust temperature.

where $I_{J,J-1}$ is the line intensity, $r_{J+1,1}$ is the line intensity ratio, and $J = 1, \ldots 7$.

For the adiabatic phase ($t < 7.5$ Myr), strong winds and supernova explosions compress the gas in the fast expanding shell to a high density $n(\mathrm{H_2}) > 10^4$ cm^{-3} (see Fig. 3), and the strong FUV radiation $G_0 > 10^4$ heats up the gas and dust of the shell to a temperature >100 K (see Fig. 4). A significant amount of highly excited CO line emission is generated from the shell and its parent cloud, and therefore the line ratios of r_{21} through r_{71} are $\geq$1.0. At around 10 Myr, all line ratios ($1 \leq J \leq 7$) have dropped below 1.0, the shell has entered the snowplow phase, the corresponding FUV field G_0 is $\leq 10^4$, the shell density $n(\mathrm{H_2})$ is $<3.0 \times 10^3$ cm^{-3}, and the gas temperature in the shell T_{gas} is between 20 and 230 K.

The far-infrared fine-structure lines are the most important cooling lines of the ISM in a galaxy. Figure 7 shows the modeling results of the line intensity ratio of [C II] 158 μm to [C I] 610 μm and the line flux ratio of [C II] 158 μm to CO(1–0). About 75% of the [C II] 158 μm emission comes from PDRs, and 25% comes from the H II region (Colbert et al. 1999). The latter is not taken into account in our calculations. The [C II] 158 μm/CO(1–0) line flux ratio rises from about 10 to 10^4 after 1 Myr, and then slowly decreases to $\sim 10^3$ at 80 Myr. It is clear that the cooling of the swept-up gas in the expanding shell is dominated by C^+; the contribution of the CO cooling is a small fraction of the total gas cooling in a massive star-forming environment.

4. APPLICATION TO THE NEARBY STARBURST GALAXY M82

In § 4.1, we compare our modeling results with the observations of an expanding supershell in the nearby starburst galaxy M82. In § 4.2 we compare our modeling results with the average gas properties in the central 1.0 kpc region of this galaxy.

M82 is an irregular starburst galaxy located at a distance of about 3.25 Mpc. This galaxy has been observed over a wide range of wavelengths. The starburst activity in M82 was likely triggered by tidal interaction with its companion M81 beginning about 10^8 yr ago in the nucleus and is currently propagating into the molecular rings. The infrared luminosity of M82 is about 4×10^{10} $L_\odot$, arising mostly from the central $\sim$400 pc region, which has a stellar bar structure and currently has a high supernova rate of $\sim$0.05–0.1 yr^{-1} (Muxlow et al. 1994). The evolutionary scheme in M82 remains under debate. The most common suggested ages of the M82 starburst in the central regions are 3–7 Myr, predicted by Colbert et al. (1999) using one instantaneous burst model in dusty media with a 100 $M_\odot$ cutoff, and 10–30 Myr, predicted by Efstathiou et al. (2000) using models of two instantaneous bursts in dusty media with a 125 $M_\odot$ cutoff. Recently, Förster-Schreiber et al. (2003) presented a more complete evolutionary scheme of the global starburst activity in M82 and suggested that there are two bursts: one occurred at $\sim$5 Myr ago, and another one at $\sim$10 Myr ago, also using instantaneous burst models in dusty media with a 100 $M_\odot$ cutoff.

4.1. *The Supershell Surrounding SNR 41.9+58*

Observations have detected an expanding supershell centered around the bright SNR 41.9+58 in both molecular line and radio continuum (Weiss et al. 1999; Wills et al. 1999). This supershell has a diameter of $\sim$130 pc, an expansion velocity of $\sim$45 km s^{-1}, and a mass of $\sim 8 \times 10^6$ $M_\odot$. Using the set of initial cloud conditions selected for our simulation (see § 3), i.e., a cloud mass $M_{\mathrm{GMC}} = 10^7$ $M_\odot$, cloud density $n_0 = 300$ cm^{-3}, ambient ISM

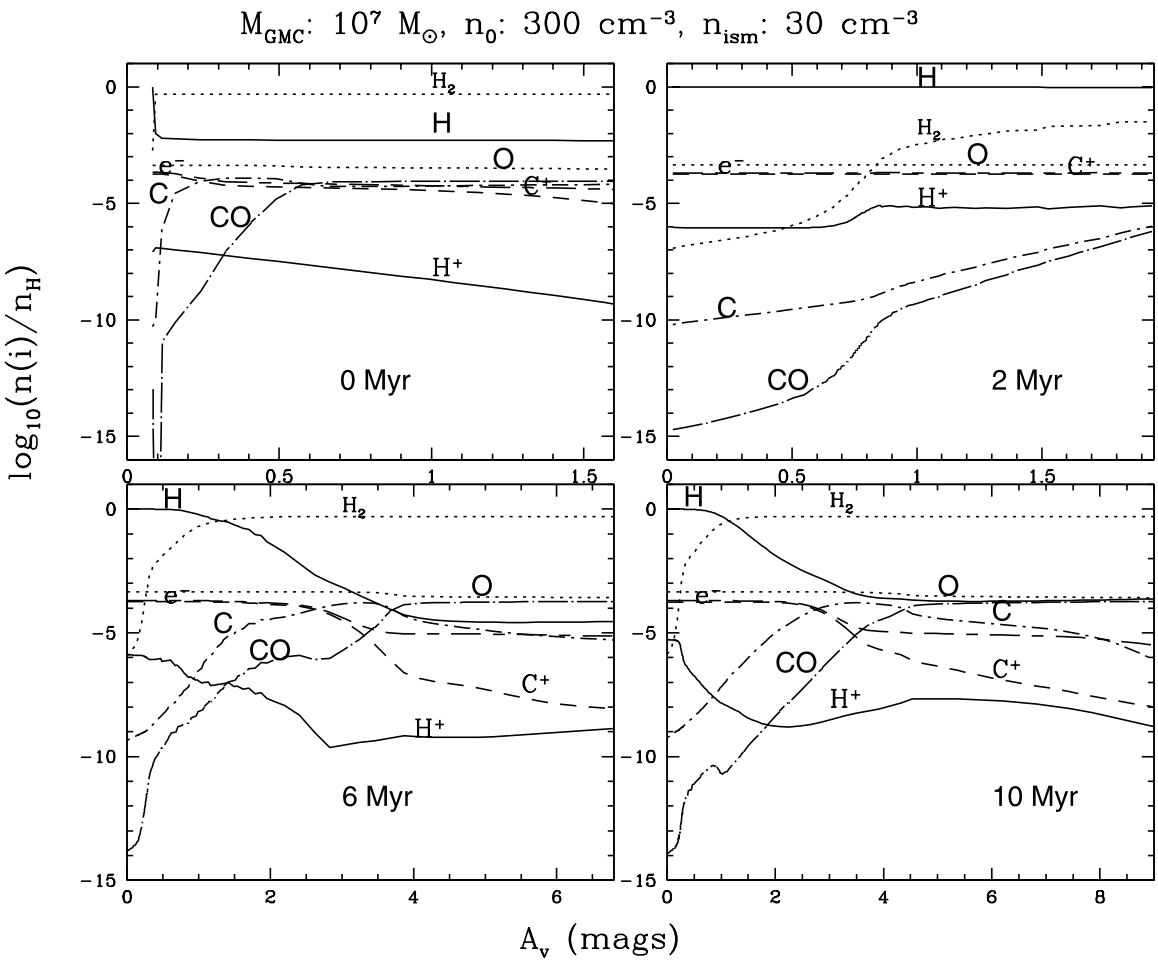

FIG. 5.—Time-dependent chemical abundances of the main species (H, H_2, H^+, e^-, C, C^+, O, and CO) relative to the total hydrogen density, as a function of visual extinction A_V for an expanding shell.

density $n_{\rm ISM} = 30$ cm^{-3}, and star formation efficiency $\eta = 0.25$, we derive a swept-up shell that has characteristics very similar to the observed one. At the observed radius of ~65 pc, our model indicates an age of 1 Myr, an expansion velocity of ~45 km s^{-1}, and a swept-up H_2 mass of $\sim 7.6 \times 10^6$ $M_\odot$. The kinetic energy of the observed supershell is estimated to be about 1.6×10^{53} ergs (Weiss et al. 1999). Our model predicts a kinetic energy of

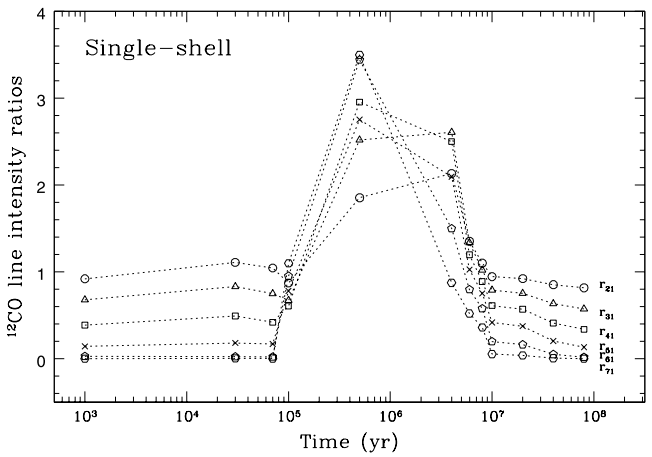

FIG. 6.—Plot of the model ^{12}CO line intensity ratios of high-J transitions to the 1–0 transition as a function of starburst age for an expanding shell. The ^{12}CO line intensities are compared in units of K km s^{-1}.

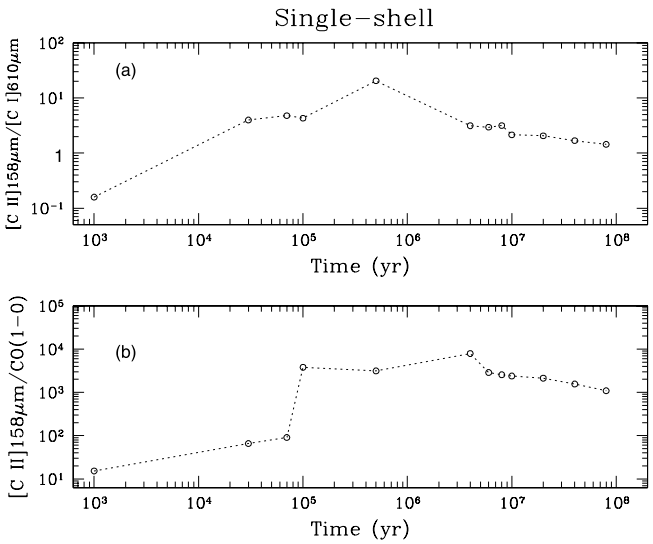

FIG. 7.—Plots of (*a*) the model line intensity ratio of [C II] 158 μm to [C I] 610 μm as a function of time (the line intensities are compared in units of K km s^{-1}) and (*b*) the model line flux ratio of [C II] 158 μm to CO(1–0) as a function of time (the fluxes are compared in units of ergs cm^{-2} s^{-1}).

TABLE 3
CHARACTERISTICS OF THE EXPANDING SUPERSHELL IN M82

Parameter	Observation	Model
Radius (pc)	65.0	65.0
Age (Myr)	1.0	1.0
Expansion velocity (km s^{-1})	45	45
Total H_2 molecular gas mass ($\times 10^6\ M_\odot$)	8.0	7.6
Kinetic energy ($\times 10^{53}$ ergs)	1.6	1.5
Total stellar mass in the center cluster ($\times 10^6\ M_\odot$)	...	2.5
Total number of O stars ($\geq 40\ M_\odot$)	...	1700
Total mechanical energy ($\times 10^{54}$ ergs)	...	1.7

$\sim 1.5 \times 10^{53}$ ergs for the expanding shell at the age of 1 Myr. The total mechanical energy needed for the creation of this supershell is $\sim 1.7 \times 10^{54}$ ergs, which is contributed by winds and supernovae associated with $\sim$1700 O stars ($\geq 40\ M_\odot$). Therefore, about 10% of the total energy is present in the form of kinetic energy of the expanding shell. The remarkably good agreement between our model results and the observations implies that this supershell may be created by strong winds and supernova explosions from a star cluster with a total mass of $2.5 \times 10^6\ M_\odot$, which occurred in the center about 1 Myr ago. The comparison is summarized in Table 3.

Furthermore, our model predictions of the CO, [C I], and [C II] line ratios for this expanding supershell can be used as a comparison with future observations, and also to constrain the physical conditions of the gas in the shell (see Figs. 6 and 7, presented in § 3.2). The model line ratios that are greater than 1.0 at $t < 8$ Myr imply that the molecular CO is optically thin in the expanding supershell. Therefore, it is better to look at the high CO transitions ($J > 3$) in this supershell.

4.2. *The Central Starburst Region*

Besides the known expanding supershell centered around SNR 41.9+58, there are other undetected shells with sizes ranging from several tens of parsecs to more than 1 kpc, and kinetic energies ranging from $\sim 10^{50}$ ergs to more than 10^{54} ergs. These shells would likely be present as partial arcs, or fragments, or cloudlike clumps due to strong winds and supernova explosions or due to shell-shell and shell-cloud interactions; only a few are visible as full circular arcs. The very good agreement between our model and the supershell observations indicates that the set of models we have put forward in this paper can be used to interpret other shells in a starburst galaxy such as M82. In this section, we illustrate the possibilities by comparing our model calculations with the observed FIR/submm/mm properties of molecular and atomic line emission in the central starburst regions.

First of all, Figure 8 shows the model ratio-ratio plots of HCN (4–3)/(3–2) versus HCN (3–2)/(1–0) and HCO^+(4–3)/(3–2) versus HCO^+(3–2)/(1–0), and a comparison with the observations of dense gas in the central 300 pc region (Seaquist & Frayer 2000). The dense gas tracers HCN and HCO^+ are better indicators of active star formation than CO, but poor tracers of the total molecular gas content. For both plots, the best agreement is at a starburst age of $\sim$3 Myr, implying that the expanding shell size is about 300 pc. Second, Figure 9 shows the model ratio-ratio plots for ^{12}CO and ^{13}CO, and a comparison with the observations of the CO line emission from three lobes (northeast, center, and southwest) in the central 300–600 pc regions (Mao et al. 2000). The isotope abundance ratio [^{12}CO]/[^{13}CO] is adopted to be 75 for the simulation. The best agreement shown in panels (*a*), (*b*), and (*d*) is at a starburst age of $\sim$6 Myr, and $\sim$3 Myr for panel (*c*), corresponding to shell sizes between 300 and 560 pc. The physical conditions for the gas of the shell at age 3–6 Myr are $G_0 \sim (2\text{–}15) \times 10^4$, $n(H_2) \sim (1.0\text{–}2.0) \times 10^4$ cm^{-3}, $T_{gas} \sim 50\text{–}250$ K, and total molecular gas mass $M_{mol} \sim (0.3\text{–}2.1) \times 10^8\ M_\odot$. Finally, Figure 10 shows the model ratio-ratio diagram of [O I] 63 μm/[C II] 158 μm versus [O I] 63 μm/[O I] 145 μm, and a comparison with the observations of these atomic lines from the central 1.1 kpc region (Negishi et al. 2001). The model [C II] 158 μm line is underestimated by a factor of about 1.3, since about 25% of the total line emission coming from the H II region is not included in the calculation. Therefore, the best agreement between the model and the observation is achieved at an age of $\sim$25 Myr old. The atomic line data are based on an 80″ beam, whereas the molecular line data pertain only to the lobes and nuclear sources at a 22″ beam. Thus, part of the reason for the discordant age in the atomic data may be the different regions sampled, since they may have a different starburst history. Our predicted gas conditions for the shell at this age are $G_0 \sim 500$, $n(H_2) \sim 1.8 \times 10^3$ cm^{-3}, $T_{gas} > 15$ K, and $M_{mol} \sim 6.0 \times 10^8\ M_\odot$. These conditions are consistent with the PDR model fits to the observations by Colbert et al. (1999). But the age inferred by Colbert et al. (1999) is 3–7 Myr. The large age discrepancy between the two different modeling results from the fact that our model includes a more massive cluster that then

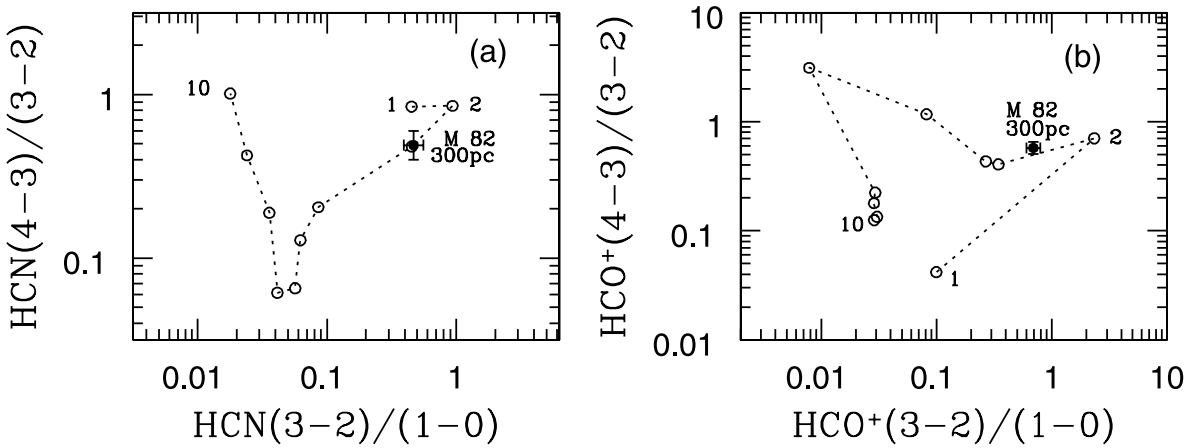

FIG. 8.—Ratio-ratio diagrams of the HCN and HCO^+ line intensities. Plots of (*a*) the model HCN(4–3)/(3–2) line ratio vs. the HCN (3–2)/(1–0) ratio for the sequence of starburst ages 0, 0.03, 2, 6, 10, 20, 30, 40, 50, and 70 Myr (labeled 1, 2, . . . 10); and (*b*) the model HCO^+(4–3)/(3–2) line ratio vs. the HCO^+(3–2)/(1–0) ratio for a sequence of starburst ages 0.03, 0.7, 2, 4, 10, 20, 30, 40, 50, and 70 Myr (labeled 1, 2, . . . 10). The modeling results are indicated by the open circles connected with dotted lines. The filled circles with error bars in the plots are the observed data (see text for details).

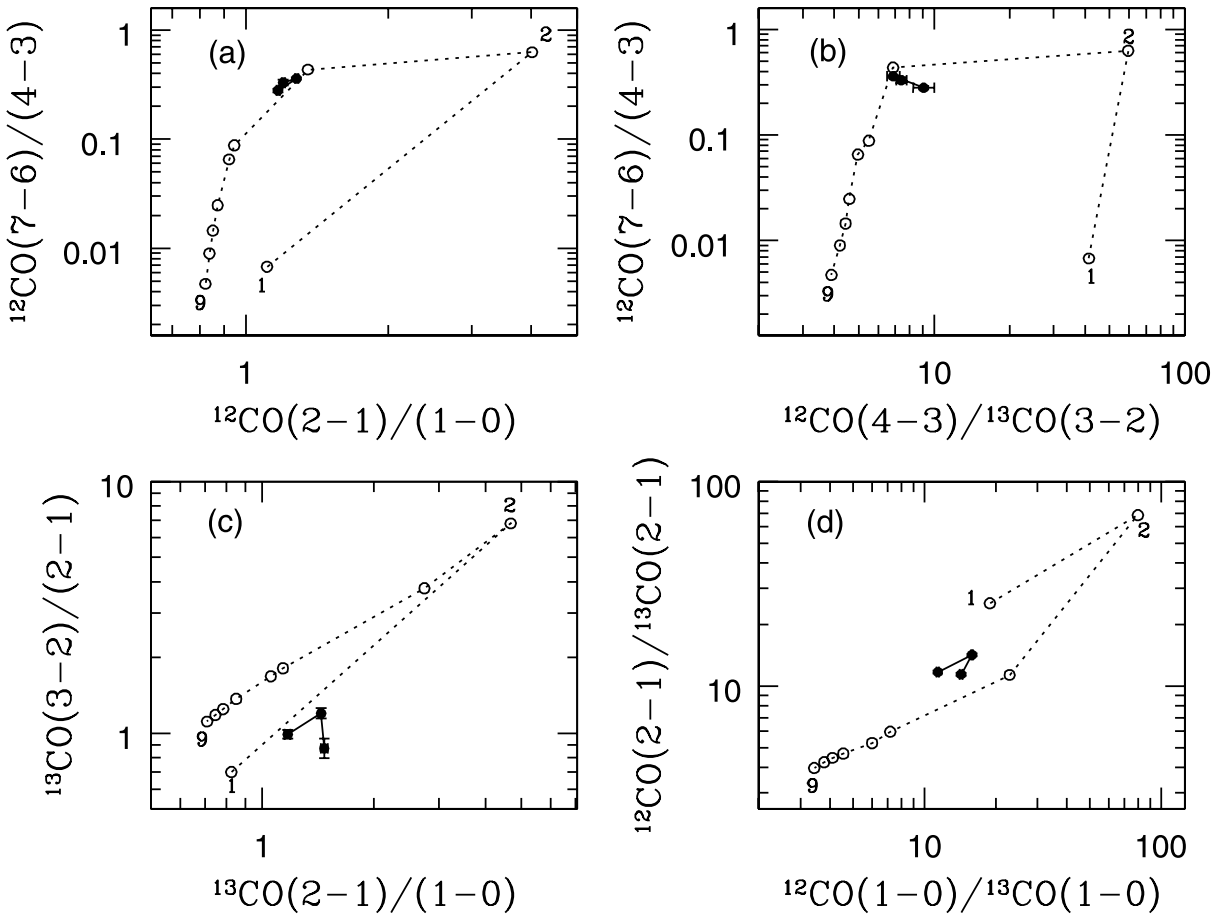

FIG. 9.—Ratio-ratio diagrams of the ^{12}CO and ^{13}CO line intensities. The modeling results for the sequence of starburst ages 0.03, 4, 6, 10, 20, 30, 40, 50, and 70 Myr (labeled 1, 2, . . . 9) are indicated by the open circles connected with dotted lines. The filled circles connected by solid lines show the observed data for the three lobes in the center of M82 (see text for details).

yields the same gas conditions (FUV flux and gas density) at a larger distance and hence, in the context of an expanding shell, an older age. It is clear that the starburst age of the whole central region is model-dependent. More simulations with a variety of input cloud conditions and a comparison with data taken at a wider range of wavelengths are needed in order to identify the ages of starbursts accurately.

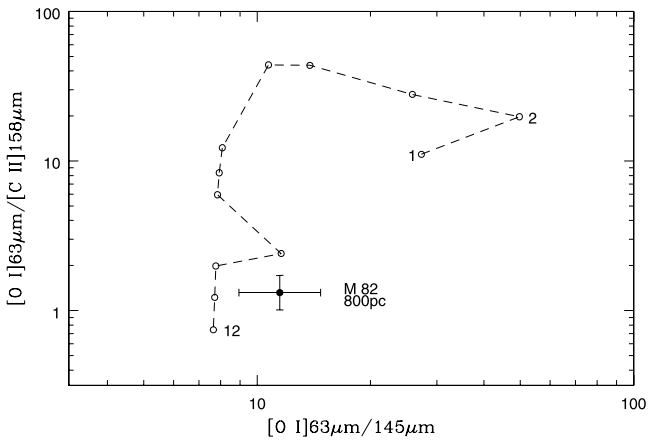

FIG. 10.—Ratio-ratio diagram of the fine-structure line fluxes. The model [O I] 63 μm/[C II] 158 μm ratio vs. [O I] 63 μm/145 μm ratio for the sequence of starburst ages 0, 0.03, 0.07, 0.1, 0.7, 4, 6, 8, 10, 20, 40, and 80 Myr (labeled 1, 2, . . . 12); the line fluxes are compared in units of W m^{-2}. The modeling results are indicated by the open circles connected with dashed lines. The filled circle shows the observed data for M82.

Although different stages of development are applicable to different central regions of M82, the shell sizes and the physical conditions of the gas within the rings (diameter ∼300–600 pc) predicted by our model are similar to what is expected from models involving expanding shells from a central starburst such as those proposed by Carlstrom & Kronberg (1991). Therefore, it is possible that the molecular rings in M82 are a product of gas that was swept up by the nuclear starburst activity that has evolved for about 10^8 yr. Their hypothesis is supported by the observations of CO line emission and continuum emission, as well as by the discovery of supershells that have not yet had time to break out of the galactic plane of M82. However, it is important to realize that the foregoing interpretation of the lobes as a ring or torus is not unique. A number of authors have argued that the molecular rings may be a product of Linblad resonance instabilities associated with the gravitational effects of the bar (e.g., Shen & Lo 1996; Wills et al. 2000). In future work, we will carry out more simulations to test the hypothesis suggested by Carlstrom & Kronberg (1991).

5. CONCLUSIONS

We have presented a set of starburst models that can be used to relate the observed FIR/submm/mm properties of molecular and atomic gas in a starburst galaxy to its age and star formation history. As a preliminary approach, we have illustrated our model

by a comparison with the observations of the expanding supershell centered around SNR 41.9+58. The very good agreement implies that the expanding supershell is created by strong stellar winds and SN explosions from a young star cluster ($\sim 2.5 \times 10^6\ M_\odot$) located in its center.

Our model predictions of CO, HCN, and HCO^+ line ratios agree with the molecular data for the central lobes (300–600 pc) for a shell with an age in the 3–7 Myr range. This implies that the molecular rings are possibly a consequence of swept-up or compressed gas caused by massive star formation originating in the nucleus of M82. More simulations in future work may be able to justify this hypothesis. The atomic line ratios calculated by our model do not fit the observed data as well as the molecular data, but suggest a much older shell, because the atomic line emission comes from a much larger region (>1 kpc). A variety of modeling parameters need to be considered to yield more accurate starburst ages.

Our model also yields appropriate values for the gas density, temperature, and structure scales compared to those measured in the center of M82 (e.g., Lynds & Sandage 1963; Nguyen et al. 1989; Stutzki et al. 1997; Seaquist & Frayer 2000; Mao et al. 2000; Negishi et al. 2001; Ward et al. 2003), and the total H_2 content within the inner 600 pc ($\sim 2.0 \times 10^8\ M_\odot$) is compatible with the observations (e.g., Wild et al. 1992). Therefore, the neutral ISM in the central star-forming region of M82 may be viewed as a product of evolving shells and is now presenting itself in the form of fragments, small cloud clumps, sheets, or even full circular arcs.

L. Y. would like to thank Andreas Efstathiou, Claus Leitherer, and Peter van Hoof. L. Y. is grateful to Chris Loken and Hugh Merz at the Canadian Institute for Theoretical Astrophysics for their generosity in allowing her to run the PDR simulations on their fastest PC machines. L. Y. is also grateful for use of the PPARC-funded Miracle Computing Facility, located at UCL, to perform her RT calculations. We thank the referee for helpful comments and suggestions. This research was supported by a research grant from the Natural Sciences and Engineering Research Council of Canada (to E. R. S.), and a Reinhardt Graduate Student Travel Fellowship from the Department of Astronomy and Astrophysics at the University of Toronto. T. A. B. is supported by a PPARC studentship. S. V. acknowledges individual financial support from a PPARC advanced Fellowship.

REFERENCES

Abbott, D. C. 1982, ApJ, 263, 723
Bell, T. A., Viti, S., Williams, D. A., Crawford, I. A., & Price, R. J. 2005, MNRAS, 357, 961
Bradford, C. M., Nikola, T., Stacey, G. J., Bolatto, A. D., Jackson, J. M., Savage, M. L., Davidson, J. A., & Higdon, S. J. 2003, ApJ, 586, 891
Carlstrom, J. E., & Kronberg, P. P. 1991, ApJ, 366, 422
Castor, J., McCray, R., & Weaver, R. 1975, ApJ, 200, L107
Colbert, J. W., et al. 1999, ApJ, 511, 721
Comeron, F., & Torra, J. 1994, ApJ, 423, 652
Dopita, M. A., et al. 2005, ApJ, 619, 755
Efstathiou, A., Rowan-Robinson, M., & Siebenmorgen, R. 2000, MNRAS, 313, 734
Förster-Schreiber, N. M., Genzel, R., Lutz, D., & Sternberg, A. 2003, ApJ, 599, 193
Franco, J., Tenorio-Tagle, G., & Bodenheimer, P. 1990, ApJ, 349, 126
Gao, Y., Lo, K. Y., Lee, S.-W., & Lee, T.-H. 2001, ApJ, 548, 172
Goldreich, P., & Kwan, J. 1974, ApJ, 189, 441
Hartquist, T. W., Falle, S. A. E. G., & Williams, D. A. 2003, Ap&SS, 288, 369
Hollenbach, D. J., Takahashi, T., & Tielens, A. G. G. M. 1991, ApJ, 377, 192
Hollenbach, D. J., & Tielens, A. G. G. M. 1997, ARA&A, 35, 179
Kennicutt, R. C., Jr. 1998, ApJ, 498, 541
Koo, B., & McKee, C. F. 1992, ApJ, 388, 93
Leitherer, C., et al. 1999, ApJS, 123, 3
Le Teuff, Y. H., Millar, T. J., & Markwick, A. J. 2000, A&AS, 146, 157
Lynds, C. R., & Sandage, A. R. 1963, ApJ, 137, 1005
Mac Low, M. M. 1999, in IAU Colloq. 169, Variable and Nonspherical Stellar Winds in Luminous Hot Stars, ed. B. Wolf, O. Stahl, & A. W. Fullerton (Berlin: Springer), 391
Mac Low, M. M., & McCray, R. 1988, ApJ, 324, 776
Madau, P., Pozzetti, L., & Dickinson, M. 1998, ApJ, 498, 106
Mao, R. Q., Henkel, C., Schulz, A., Zielinsky, M., Mauersberger, R., Störzer, H., Wilson, T. L., & Gensheimer, P. 2000, A&A, 358, 433
McCray, R., & Kafatos, M. 1987, ApJ, 317, 190
McCray, R., & Snow, T. P., Jr. 1979, ARA&A, 17, 213
McKee, C. F. 1999, in The Origin of Stars and Planetary Systems, ed. C. J. Lada & N. D. Kylafis (Dordrecht: Kluwer), 29
McKee, C. F., & Hollenbach, D. J. 1980, ARA&A, 18, 219
Muxlow, T. W. B., Pedlar, A., Wilkinson, P. N., Axon, D. J., Sanders, E. M., & de Bruyn, A. G. 1994, MNRAS, 266, 455
Negishi, T., Onaka, T., Chan, K.-W., & Roellig, T. L. 2001, A&A, 375, 566
Nguyen, Q-L., Nakai, N., & Jackson, J. M. 1989, A&A, 220, 57
Papadopoulos, P. P., Thi, W.-F., & Viti, S. 2002, ApJ, 579, 270
Plume, R., Jaffe, D. T., & Evans, Neal, J., II. 1992, ApJS, 78, 505
Rawlings, J. M. C., & Yates, J. A. 2001, MNRAS, 326, 1423
Rieke, G. H., Lebofsky, M. J., Thompson, R. I., Low, F. J., & Tokunaga, A. T. 1980, ApJ, 238, 24
Salpeter, E. E. 1955, ApJ, 121, 161
Sanders, D. B., Scoville, N. Z., & Solomon, P. M. 1985, ApJ, 289, 373
Scalo, J., & Chappell, D. 1999, MNRAS, 310, 1
Schöier, F. L., van der Tak, F. F. S., van Dishoeck, E. F., & Black, J. H. 2005, A&A, 432, 369
Seaquist, E. R., & Frayer, D. T. 2000, ApJ, 540, 765
Shen, J., & Lo, K. Y. 1996, in IAU Symp. 170, CO: Twenty-Five Years of Millimeter-Wave Spectroscopy, ed. W. B. Latter et al. (Dordrecht: Kluwer), 101
Solomon, P. M., Rivolo, A. R., Barrett, J., & Yahil, A. 1987, ApJ, 319, 730
Spitzer, L. 1978, Physical Processes in the Interstellar Medium (New York: Wiley)
Stutzki, J., et al. 1997, ApJ, 477, L33
Suchkov, A., Allen, R. J., & Heckman, T. M. 1993, ApJ, 413, 542
Taylor, S. D., Hartquist, T. W., & Williams, D. A. 1993, MNRAS, 264, 929
Tielens, A. G. G. M., & Hollenbach, D. 1985, ApJ, 291, 722
van Dishoeck, E. F., & Blake, G. A. 1998, ARA&A, 36, 317
van Zadelhoff, G. J., et al. 2002, A&A, 395, 373
Ward, J. S., Zmuidzinas, J., Harris, A. I., & Isaak, K. G. 2003, ApJ, 587, 171
Weaver, R., McCray, R., Castor, J., Shapiro, P., & Morre, R. 1977, ApJ, 218, 377
Weiss, A., Walter, F., Neininger, N., & Klein, U. 1999, A&A, 345, L23
Wild, W., Harris, A. I., Eckart, A., Genzel, R., Graf, U. U., Jackson, J. M., Russell, A. P. G., & Stutzki, J. 1992, A&A, 265, 447
Wills, K. A., Das, M., Pedlar, A., Muxlow, T. W. B., & Robinson, T. G. 2000, MNRAS, 316, 33
Wills, K. A., Redman, M. P., Muxlow, T. W. B., & Pedlar, A. 1999, MNRAS, 309, 395